PAPER *Special Section on Digital Signal Processing*

Fingerprint Restoration Using Digital Reaction-Diffusion System and Its Evaluation

Koichi ITO[†a)], ***Student Member***, **Takafumi AOKI**[†], ***Regular Member***, ***and*** **Tatsuo HIGUCHI**[††], ***Fellow***

SUMMARY This paper presents an algorithm for fingerprint image restoration using Digital Reaction-Diffusion System (DRDS). The DRDS is a model of a discrete-time discrete-space nonlinear reaction-diffusion dynamical system, which is useful for generating biological textures, patterns and structures. This paper focuses on the design of a fingerprint restoration algorithm that combines (i) a ridge orientation estimation technique using an iterative coarse-to-fine processing strategy and (ii) an adaptive DRDS having a capability of enhancing low-quality fingerprint images using the estimated ridge orientation. The phase-only image matching technique is employed for evaluating the similarity between an original fingerprint image and a restored image. The proposed algorithm may be useful for person identification applications using fingerprint images.

key words: *reaction-diffusion system, pattern formation, digital signal processing, digital filters, fingerprint restoration*

1. Introduction

Living organisms can create a remarkable variety of patterns and forms from genetic information. In embryology, the development of patterns and forms is sometimes called *Morphogenesis*. In 1952, Alan Turing suggested that a system of chemical substances, called *morphogens*, reacting together and diffusing through a tissue, is adequate to account for the main phenomena of morphogenesis [1]. From an engineering viewpoint, the insights into morphogenesis provide important concepts for devising a new class of intelligent signal processing algorithms inspired by biological pattern formation phenomena [2]–[4].

Recently, we have proposed a framework of *Digital Reaction-Diffusion System* (DRDS)—a discrete-time discrete-space reaction-diffusion dynamical system—for designing signal processing models exhibiting active pattern/texture formation capability [5]. In Ref. [5], we have already presented the basic idea of fingerprint enhancement/restoration using a special DRDS, called an *adaptive DRDS*, which can control the orientation of pattern formation for every pixel. Our experimental observation, however, shows that the adaptive DRDS with simple orientation estimation cannot provide enough performance for poor quality fingerprint images. Also, systematic experimental evaluation of restoration performance in terms of identification rate has not been presented yet.

In this paper, we focus on the design of an improved fingerprint restoration algorithm that combines (i) a ridge orientation estimation technique using an iterative coarse-to-fine processing strategy and (ii) an adaptive DRDS having a capability of generating the most likely fingerprint pattern using the estimated ridge orientation. The restoration capability of the new algorithm is evaluated by using the phase-only matching technique [6], which has already been applied to practical fingerprint identification systems by the authors' group [7]. The coarse-to-fine orientation estimation technique directly coupled with DRDS pattern formation dynamics makes possible significant improvement in fingerprint identification performance. The new algorithm is useful for identifying a person even from a blurred fingerprint image and could enhance the performance of conventional fingerprint identification systems.

So far, there are few works on the restoration of original fingerprint patterns from incomplete fingerprint images. Most of the papers discuss fingerprint image enhancement rather than fingerprint restoration [8], [9]. The reported enhancement algorithms usually focus on passive image processing (without changing the original ridge characteristics) for extracting minutiae from input fingerprint images. The use of morphogenesis principle for fingerprint enhancement/restoration allows more active processing of fingerprint images, including the generation of most likely local patterns that interpolates missing fingerprint textures. This new idea was originally discussed in Ref. [2], but the presented idea was formulated with differential equations and was applied only to limited examples of fingerprint enhancement. In this paper, we present more systematic approach to the design and evaluation of a morphogenesis-based fingerprint restoration algorithm within the framework of DRDS.

This paper is organized as follows: Sect. 2 defines a general DRDS and shows an example of fingerprint enhancement using DRDS. Section 3 describes a fin-

Manuscript received November 22, 2002.
Manuscript revised March 2, 2003.
Final manuscript received April 14, 2003.
[†]The authors are with the Department of Computer and Mathmatical Sciences, Graduate School of Information Sciences, Tohoku University, Sendai-shi, 980-8579 Japan.
[††]The author is with the Department of Electronics, Tohoku Institute of Technology, Sendai-shi, 982-8577 Japan.
a) E-mail: ito@aoki.ecei.tohoku.ac.jp

gerprint restoration algorithm combining (i) a coarse-to-fine ridge orientation estimation strategy and (ii) an adaptive-DRDS pattern generator. Section 4 describes a set of experiments for evaluating restoration performance of the proposed algorithm and compares the new algorithm (with coarse-to-fine) with the original algorithm (without coarse-to-fine). In Sect. 5, we end with some conclusions.

2. Digital Reaction-Diffusion System

A Digital Reaction-Diffusion System (DRDS)—a model of a discrete-time discrete-space reaction-diffusion dynamical system—can be naturally derived from the original reaction-diffusion system defined in continuous space and time (see [5] for detailed mathematical formulation). The general DRDS can be obtained as

$$\begin{aligned}&\boldsymbol{x}(n_0+1, n_1, n_2)\\&\quad = \boldsymbol{x}(n_0, n_1, n_2) + \boldsymbol{R}(\boldsymbol{x}(n_0, n_1, n_2))\\&\qquad + \boldsymbol{D}(l * \boldsymbol{x})(n_0, n_1, n_2),\end{aligned} \tag{1}$$

where

$$\begin{aligned}\boldsymbol{x} &= [x_1, x_2, \cdots, x_M]^T,\\&\quad x_i : \text{concentration of the } i\text{-th morphogen},\\\boldsymbol{R} &= T_0 \tilde{\boldsymbol{R}} = [R_1(\boldsymbol{x}), R_2(\boldsymbol{x}), \cdots, R_M(\boldsymbol{x})]^T,\\&\quad R_i(\boldsymbol{x}) : \text{reaction kinetics for the } i\text{-th morphogen},\\\boldsymbol{D} &= diag[D_1, D_2, \cdots, D_M],\\&\quad diag : \text{diagonal matrix},\\&\quad D_i : \text{diffusion coefficient of the } i\text{-th morphogen},\end{aligned}$$

$$l(n_1, n_2) = \begin{cases} \frac{1}{T_1^2} & (n_1, n_2) = (-1, 0), (1, 0)\\ \frac{1}{T_2^2} & (n_1, n_2) = (0, -1), (0, 1)\\ -2(\frac{1}{T_1^2} + \frac{1}{T_2^2}) & (n_1, n_2) = (0, 0)\\ 0 & \text{otherwise,}\end{cases}$$

and $*$ is the spatial convolution operator defined as

$$(l * \boldsymbol{x})(n_0, n_1, n_2) = \begin{bmatrix} (l * x_1)(n_0, n_1, n_2)\\ (l * x_2)(n_0, n_1, n_2)\\ \vdots\\ (l * x_M)(n_0, n_1, n_2)\end{bmatrix} = \begin{bmatrix} \sum_{p_1=-1}^{1} \sum_{p_2=-1}^{1} l(p_1, p_2) x_1(n_0, n_1 - p_1, n_2 - p_2)\\ \sum_{p_1=-1}^{1} \sum_{p_2=-1}^{1} l(p_1, p_2) x_2(n_0, n_1 - p_1, n_2 - p_2)\\ \vdots\\ \sum_{p_1=-1}^{1} \sum_{p_2=-1}^{1} l(p_1, p_2) x_M(n_0, n_1 - p_1, n_2 - p_2)\end{bmatrix}.$$

The DRDS described by (1) can be understood as a 3-D nonlinear digital filter. We first store an initial (input) image in a specific morphogen, say $x_i(0, n_1, n_2)$, at time 0. After computing the dynamics for n_0 steps, we can obtain the output image from one of the M morphogens, say $x_i(n_0, n_1, n_2)$, at time n_0. In general, linear digital filters with guaranteed stability are widely used in many signal processing applications. In our application, however, we employ the DRDS with nonlinear reaction kinetics $\boldsymbol{R}(\boldsymbol{x})$ satisfying the diffusion-driven instability condition [5]. In this case, DRDS becomes an unstable 3-D nonlinear digital filter having significant pattern formation capability.

In this paper, we use the two-morphogen DRDS ($M = 2$) with the Brusselator reaction kinetics, which is one of the most widely studied chemical oscillators [10]. The two-morphogen Brusselator-based DRDS is defined as follows:

$$\begin{aligned}\begin{bmatrix} x_1(n_0+1, n_1, n_2)\\ x_2(n_0+1, n_1, n_2)\end{bmatrix} &= \begin{bmatrix} x_1(n_0, n_1, n_2)\\ x_2(n_0, n_1, n_2)\end{bmatrix}\\&\quad + \begin{bmatrix} R_1(x_1(n_0, n_1, n_2), x_2(n_0, n_1, n_2))\\ R_2(x_1(n_0, n_1, n_2), x_2(n_0, n_1, n_2))\end{bmatrix}\\&\quad + \begin{bmatrix} D_1(l * x_1)(n_0, n_1, n_2)\\ D_2(l * x_2)(n_0, n_1, n_2)\end{bmatrix},\end{aligned} \tag{2}$$

where

$$\begin{aligned}R_1(x_1, x_2) &= T_0 \left\{k_1 - (k_2 + 1)x_1 + x_1^2 x_2\right\},\\R_2(x_1, x_2) &= T_0(k_2 x_1 - x_1^2 x_2).\end{aligned}$$

In this paper, we employ the parameter set: $k_1 = 2$, $k_2 = 4$, $T_0 = 0.01$, $D_1 = T_0$ and $D_2 = 5T_0$ (see Appendix).

The DRDS thus defined can be used to enhance fingerprint patterns. To do this, we first set the initial fingerprint image in $x_1(0, n_1, n_2)$, at time 0. Note that spatial sampling parameters T_1 and T_2 should be adjusted according to the inherent spatial frequency of the given fingerprint image. The dynamics (2) has the equilibrium $(x_1, x_2) = (2, 2)$, and the variation ranges of variables (x_1, x_2) are bounded around the equilibrium point as $1 \leqq x_1 \leqq 3$ and $1 \leqq x_2 \leqq 3$ in the case of given parameter set. Hence, we first scale the [0,255] gray-scale fingerprint image into [1,3] range. The scaled image becomes the initial input $x_1(0, n_1, n_2)$, while the initial condition of the second morphogen is given by $x_2(0, n_1, n_2) = 2$. The zero-flux Neumann boundary condition is employed for computing the dynamics. After n_0 steps of DRDS computation, we obtain $x_1(n_0, n_1, n_2)$ as an output image, which is scaled back into the [0,255] gray-scale image to produce the final output. Figure 1 shows the enhancement of a fingerprint image using DRDS.

Our initial observation, however, shows that the DRDS with a spatially isotropic diffusion term (2) often produces some broken ridge lines in processing fingerprint images as shown in Fig. 1, since it does not

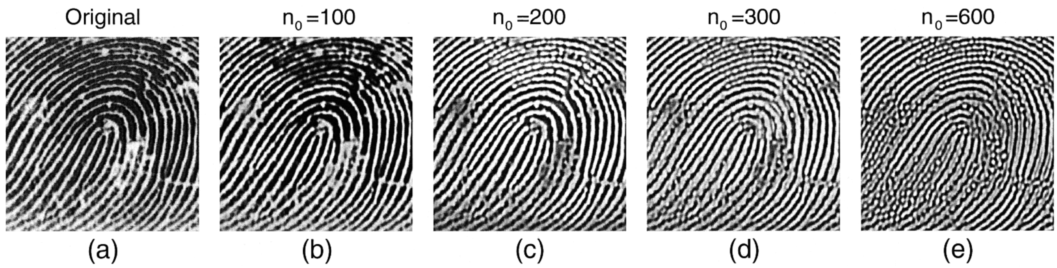

Fig. 1 Fingerprint enhancement: (a) original image, (b)–(e) enhanced images.

take account of the local orientation of ridge flow. In order to solve this problem, the next section defines an *adaptive DRDS* model, in which we can use the local orientation of the ridge flow in a fingerprint image to guide the action of DRDS. This can be realized by introducing orientation masks to be convolved with the diffusion terms in DRDS (2).

3. Fingerprint Restoration Algorithm Using Adaptive DRDS and Coarse-to-Fine Orientation Estimation

In this section, we modify the definition of the simple two-morphogen DRDS (2) to have an adaptive DRDS model dedicated to fingerprint restoration tasks. The two-morphogen adaptive DRDS with the Brusselator reaction kinetics can be written as

$$\begin{aligned}\begin{bmatrix} x_1(n_0+1, n_1, n_2) \\ x_2(n_0+1, n_1, n_2) \end{bmatrix} &= \begin{bmatrix} x_1(n_0, n_1, n_2) \\ x_2(n_0, n_1, n_2) \end{bmatrix} \\ &+ \begin{bmatrix} R_1(x_1(n_0, n_1, n_2), x_2(n_0, n_1, n_2)) \\ R_2(x_1(n_0, n_1, n_2), x_2(n_0, n_1, n_2)) \end{bmatrix} \\ &+ \begin{bmatrix} D_1(h_1^{n_1 n_2} * l * x_1)(n_0, n_1, n_2) \\ D_2(h_2^{n_1 n_2} * l * x_2)(n_0, n_1, n_2) \end{bmatrix}, \end{aligned} \quad (3)$$

where $h_i^{m_1 m_2}(n_1, n_2)$ is an orientation mask at the pixel (m_1, m_2) for the i-th morphogen.

The orientation mask $h_1^{m_1 m_2}(n_1, n_2)$ at the pixel (m_1, m_2) is a 32×32 matrix of real coefficients defined within the window $(n_1, n_2) = (-16, -16) \sim (15, 15)$. The mask $h_1^{m_1 m_2}(n_1, n_2)$ controls the dominant orientation of the generated pattern at every pixel (m_1, m_2) depending on the local ridge flow in the given fingerprint image. Figure 2 shows the 180 distinct orientation masks used in our system corresponding to the discrete angles from 0° to 179°.

The orientation mask having the angle θ is calculated as illustrated in Fig. 3. Within the 32×32 window in frequency domain, we define a mask pattern $H_1^{m_1 m_2}(j\omega_1, j\omega_2)$ for the angle θ as shown in Fig. 3, where

$$H_1^{m_1 m_2}(j\omega_1, j\omega_2) = \begin{cases} 1 & \text{for unstable frequency band} \\ & \text{(black pixels in Fig. 3(a))}, \\ 2 & \text{otherwise.} \end{cases}$$

The orientation mask $h_1^{m_1 m_2}(n_1, n_2)$ for the angle θ (shown in Fig. 3(b)) is obtained as an inverse Fourier transform of $H_1^{m_1 m_2}(j\omega_1, j\omega_2)$. The orientation mask $h_2^{m_1 m_2}(n_1, n_2)$ for the second morphogen, on the other hand, has the value 1 at the center $(n_1, n_2) = (0, 0)$, and

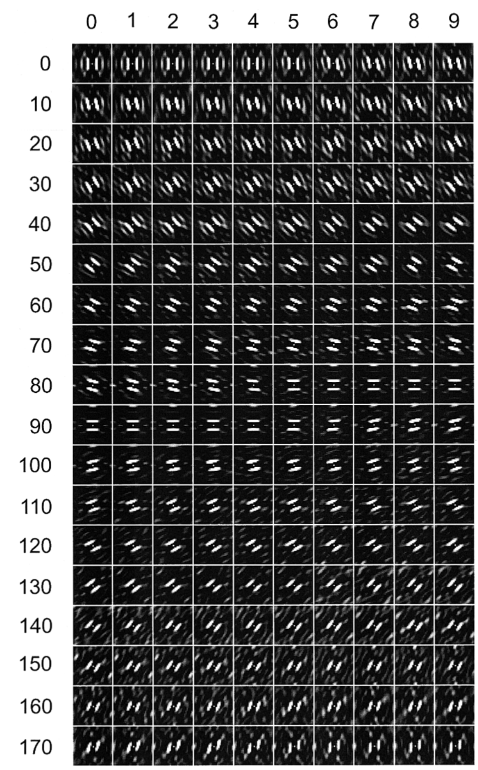

Fig. 2 180 orientation masks used in our experiments.

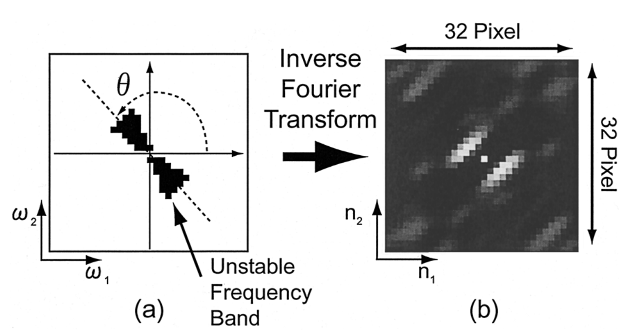

Fig. 3 Orientation mask for angle θ shown in (a) frequency domain (ω_1, ω_2), and in (b) space (n_1, n_2).

```
procedure Adaptive DRDS with Hierarchical Orientation Estimation
begin
  p := 2; { initialize the image partitioing factor}
  while time step n0 equals to 500 do
  begin
    if p is less than 10 then
    begin
      partition the input image into p^2 sub-images;
      select independent orientation masks for
      p^2 sub-images;
      run the adaptive DRDS (Eq. (3)) for
      10 time steps;
      p := p + 1
    end
    else
    begin
      select independent orientation masks
      for all pixels;
      run the adaptive DRDS (Eq. (3)) for
      10 time steps
    end
  end
end.
```

Fig. 4 Fingerprint restoration algorithm with coarse-to-fine orientation estimation.

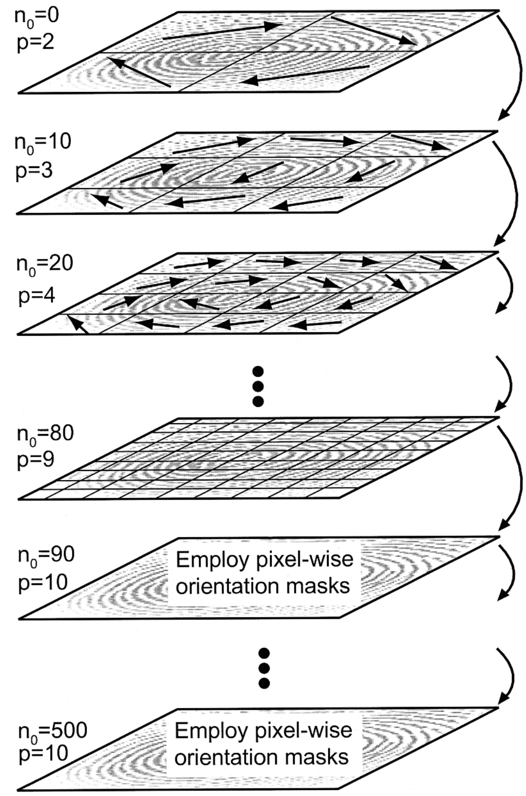

Fig. 5 Coarse-to-fine orientation estimation scheme.

equals to 0 for other coordinates (n_1, n_2). Thus, the dynamics for the morphogen $x_2(n_0, n_1, n_2)$ does not take account of the local orientation.

In Ref. [5], we have presented the basic idea of fingerprint enhancement/restoration using the adaptive DRDS. For fingerprint restoration, we first detect the dominant orientation θ of local ridge flow at every pixel (m_1, m_2) in a given fingerprint image. Then, we select the mask pattern corresponding to the angle θ in Fig. 2 as $h_1^{m_1m_2}(n_1, n_2)$. In our experiment, we employ the Fourier transform of a local fingerprint image to estimate its dominant orientation. Our experimental observation, however, shows that the adaptive DRDS with simple orientation estimation strategy cannot provide enough performance for poor quality fingerprint images.

Addressing this problem, we introduce a ridge orientation estimation technique using an recursive coarse-to-fine processing strategy. The computation flow of the proposed restoration algorithm is described in Fig. 4. As illustrated in Fig. 5, we first partition the fingerprint image into p^2 sub-images, where the initial value of p is 2, and select p^2 different orientation masks for p^2 sub-images independently by estimating dominant ridge orientation in each sub-image. Note that the pixels within a common sub-image employ the same orientation mask $h_1^{m_1m_2}(n_1, n_2)$. Using the obtained orientation masks, we run the adaptive DRDS for 10 steps ($n_0 = 0 \sim 9$) to interpolate the incomplete fingerprint pattern. After incrementing the image partitioning factor p (i.e., $p = 3$), we perform the same tasks (i.e., ridge orientation estimation and pattern reshaping by adaptive DRDS for $n_0 = 10 \sim 19$) in every sub-image. This process is repeated by incrementing the image partitioning factor p until $p = 9$ ($n_0 = 20 \sim 89$). For $p > 9$, we estimate pixel-wise local orientation, give distinct orientation masks for all the pixels, and run the adaptive DRDS for 10 steps. This process is carried out until $n_0 = 500$ by updating orientation masks in every 10 steps. The proposed algorithm gradually increases the precision of pattern formation instead of going directly into pixel-wise orientation control. This recursive strategy makes possible significant improvement in the quality of restored fingerprint images.

4. Experiments and Discussion

This section describes a set of experiments for evaluating restoration performance of the proposed algorithm. The problem considered here is to restore the original fingerprint image from its "subsampled" image. For this purpose, we generate a subsampled fingerprint image from the original image as follows (see Fig. 6): (i) partition the original image into $R \times S$-pixel rectangular blocks, and (ii) select one pixel randomly from every block and eliminate all the other pixels (set 127, middle gray-level, to the pixels). The image thus obtained has the same size as the original image, but the number of effective pixels is reduced to $1/(R \times S)$.

The restoration capability of the proposed algorithm is evaluated by calculating the similarity between the original fingerprint image and the restored image. To measure the similarity, we employ the phase-only image matching technique [6] (illustrated in Fig. 7), which has been proved to have an efficient discrimination capability in practical fingerprint identification tasks. In this experiment, we capture 15 distinct fingerprint images (Finger01–Finger15) from 15 persons using a fingerprint recognition system (Yamatake Corporation, "FriendTouch System" [7]). The captured image size is 256×256. Restoration experiments are carried out for various subsampling rates: $1/(3 \times 3)$, $1/(3 \times 4)$, $1/(4 \times 4)$, $1/(4 \times 5)$, $1/(5 \times 5)$, $1/(5 \times 6)$, $1/(6 \times 6)$, $1/(6 \times 7)$, $1/(7 \times 7)$, $1/(7 \times 8)$ and $1/(8 \times 8)$.

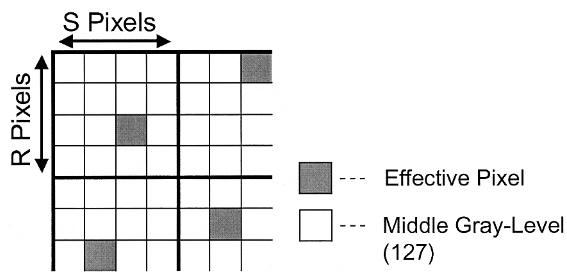

Fig. 6 $1/(R \times S)$ subsampling.

In the following, we focus on the result of restoration from $1/(4\times4)$-, $1/(5\times5)$- and $1/(6\times6)$-subsampled images, for example. Figures 8, 9 and 10 show the restoration of fingerprint images from the subsampled images, where the subsampling rate is $1/(4\times4)$, $1/(5\times5)$ and $1/(6\times6)$, respectively. Every figure includes the original image, the subsampled image ($n_0 = 0$) and restored images at $n_0 = 100$, 200 and 400, respectively. We can observe that the fingerprint pattern is reconstructed from the subsampled image gradually as time step n_0 increases. Figure 11 shows the restoration of fingerprint image from the $1/(6 \times 6)$ subsampled image without employing coarse-to-fine processing, for comparison. Figure 12 shows the visualized orientation of ridge flow for the case of $1/(6 \times 6)$ subsampling. It is difficult to estimate the correct orientation information from the subsampled image as shown in Fig. 12(b). Figures 12(c)–(l) show the estimated orientation using the coarse-to-fine technique described in the last section. Figure 12(l) shows that the estimated orientation

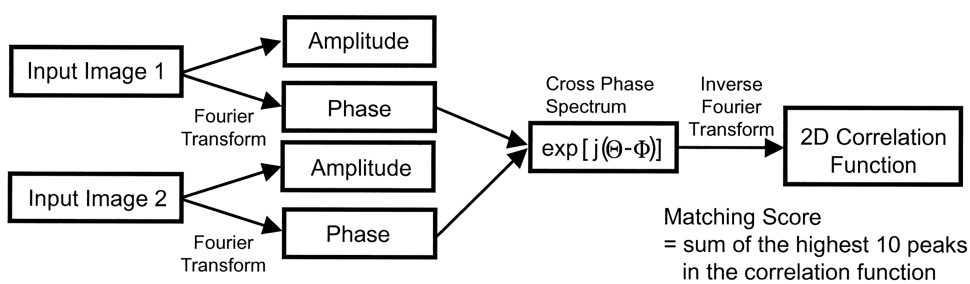

Fig. 7 Phase-only matching technique.

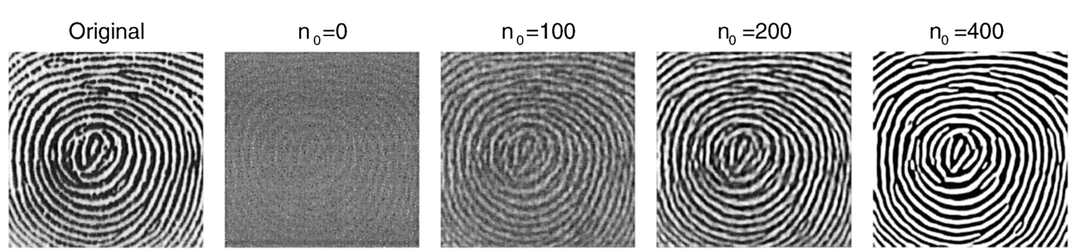

Fig. 8 Fingerprint image restoration from a $1/(4 \times 4)$-subsampled image of *Finger01*.

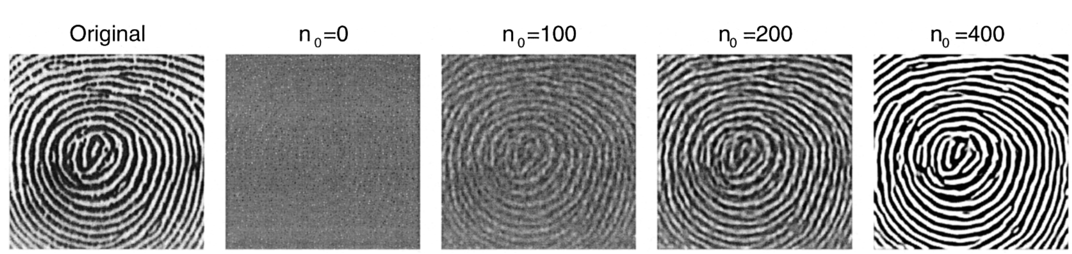

Fig. 9 Fingerprint image restoration from a $1/(5 \times 5)$-subsampled image of *Finger01*.

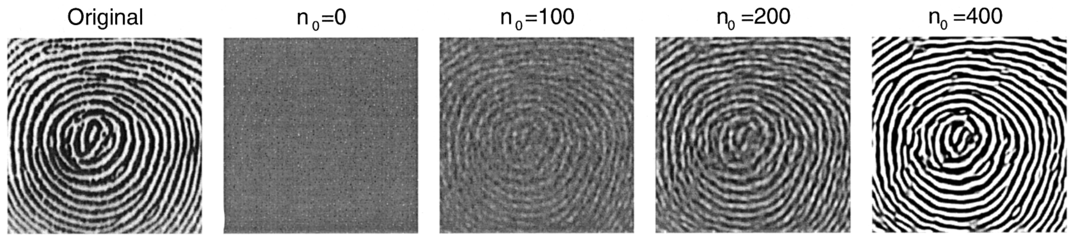

Fig. 10 Fingerprint image restoration from a $1/(6 \times 6)$-subsampled image of *Finger01*.

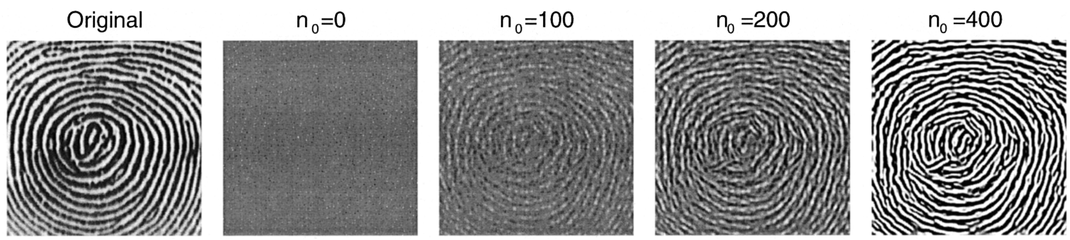

Fig. 11 Fingerprint image restoration from a $1/(6 \times 6)$-subsampled image of *Finger01* without coarse-to-fine processing.

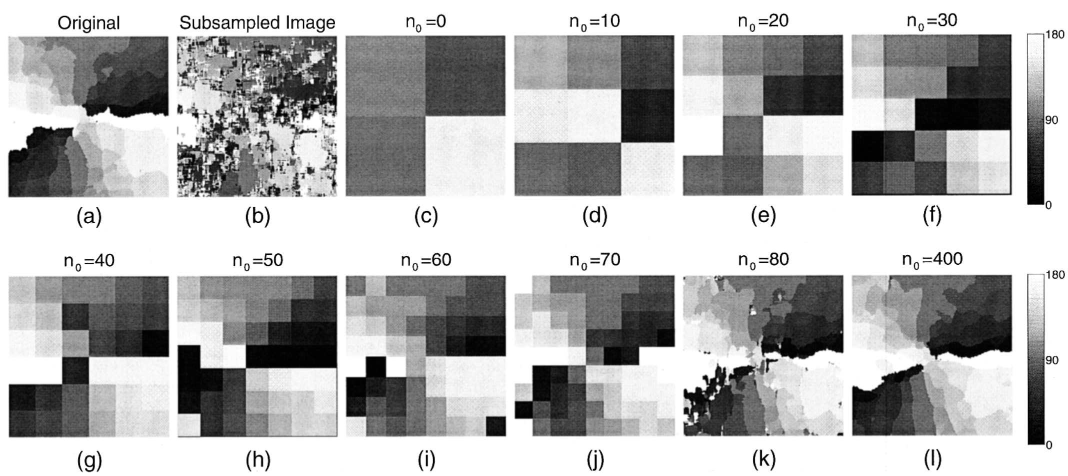

Fig. 12 Visualized orientation of ridge flow in *Finger01*: (a) original image, (b) $1/(6 \times 6)$-subsampled image, (c)–(l) restored images (estimated angle θ).

information after $n_0 = 400$ is very close to the original information (Fig. 12(a)). Using the orientation information thus obtained, the adaptive DRDS can restore the pattern of Finger01 correctly.

Figures 13, 14 and 15 show the variation of matching scores between the original image of Finger01 and the restored images of Finger01–Finger15 for the case of subsampling rate: $1/(4\times4)$, $1/(5\times5)$ and $1/(6\times6)$, respectively. The matching score of the restored image of Finger01 increases selectively as the number of steps n_0 increases. For every experimental trial, the optimal discrimination capability is obtained around $n_0 = 400$, which is indicated with a vertical dashed line in every figure. The horizontal dashed line indicates the threshold for fingerprint discrimination, where we employ the threshold value 0.5. In the range of $n_0 = 200 \sim 300$, the

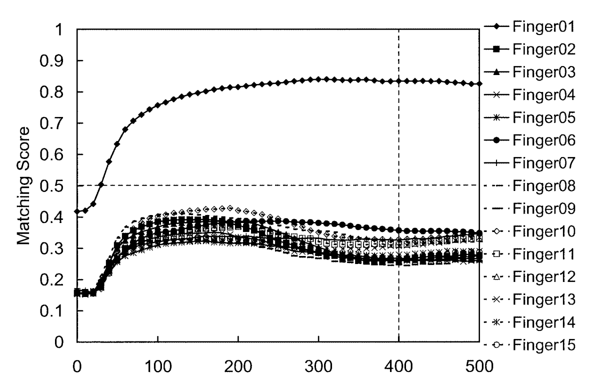

Fig. 13 Matching scores between the original image of *Finger01* and the restored images of Finger01–Finger15 (restoration from $1/(4 \times 4)$-subsampled images).

matching score for the wrong fingerprints drop gradually while the correct fingerprint keeps sufficient level of matching score.

Tables 1, 2 and 3 summarize matching scores (at $n_0 = 400$) between original and restored images of Finger01–Finger15 for subsampling rates $1/(4 \times 4)$, $1/(5 \times 5)$ and $1/(6 \times 6)$, respectively. For these cases, auto-correlation exhibits significantly higher scores than the cross-correlation scores. Thus, we can confirm that the proposed algorithm restores the original fingerprint patterns from subsampled images of Finger01–15 completely for subsampling rates $1/(4 \times 4)$, $1/(5 \times 5)$ and $1/(6 \times 6)$.

Table 4 compares the success rate of fingerprint identification between the restoration algorithms with and without coarse-to-fine processing for various subsampling rates. The original algorithm achieves 100% identification up to $1/(4 \times 4)$ subsampling. On the other hand, the proposed algorithm employing coarse-to-fine processing can completely restore the original fingerprint pattern up to the subsampling rate $1/(6 \times 6)$. This experiment demonstrates a potential capability of adaptive DRDS with coarse-to-fine approach to enhance the performance of matching algorithms

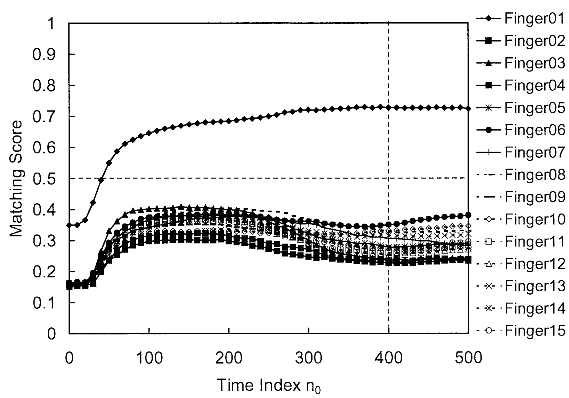

Fig. 14 Matching scores between the original image of *Finger01* and the restored images of Finger01–Finger15 (restoration from $1/(5 \times 5)$-subsampled images).

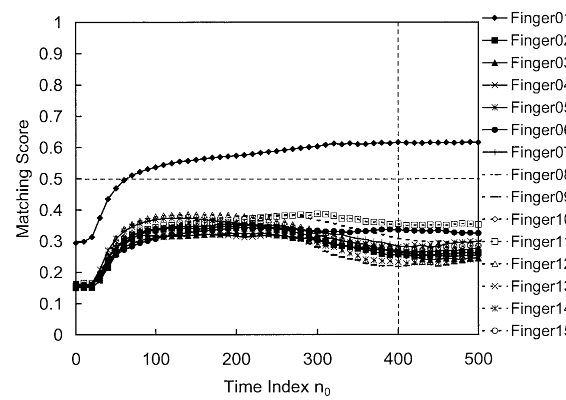

Fig. 15 Matching scores between the original image of *Finger01* and the restored images of Finger01–Finger15 (restoration from $1/(6 \times 6)$-subsampled images).

Table 1 Matching scores at $n_0 = 400$ (restoration from $1/(4 \times 4)$-subsampled images).

		Original Image														
		Finger01	Finger02	Finger03	Finger04	Finger05	Finger06	Finger07	Finger08	Finger09	Finger10	Finger11	Finger12	Finger13	Finger14	Finger15
Restored Image	Finger01	**0.8342**	0.2573	0.2614	0.2675	0.2608	0.3566	0.3259	0.3206	0.2477	0.3285	0.3110	0.2691	0.3069	0.2793	0.2659
	Finger02	0.2464	**0.7924**	0.3097	0.2449	0.3059	0.3666	0.3079	0.2783	0.2547	0.2503	0.2934	0.2630	0.2629	0.2786	0.2901
	Finger03	0.2617	0.2658	**0.7725**	0.2850	0.2787	0.3738	0.2993	0.2938	0.2635	0.2568	0.2530	0.2993	0.3171	0.2915	0.3049
	Finger04	0.2559	0.2676	0.2743	**0.8166**	0.2676	0.3836	0.3467	0.2947	0.2786	0.2640	0.3354	0.3250	0.2791	0.3167	0.2817
	Finger05	0.2587	0.2767	0.2515	0.2841	**0.7215**	0.4677	0.3375	0.3091	0.2966	0.2734	0.2886	0.3256	0.3512	0.2770	0.2717
	Finger06	0.2427	0.2284	0.2622	0.2990	0.2869	**0.7604**	0.3830	0.3067	0.2538	0.2898	0.2732	0.2779	0.3779	0.2967	0.2841
	Finger07	0.2702	0.2600	0.2971	0.2695	0.2795	0.3927	**0.7596**	0.3035	0.2522	0.2551	0.3269	0.2957	0.2745	0.2409	0.2689
	Finger08	0.3387	0.3102	0.2667	0.2911	0.2909	0.4014	0.3515	**0.7761**	0.2488	0.2600	0.3000	0.3257	0.3430	0.2856	0.3028
	Finger09	0.2598	0.2421	0.2526	0.2395	0.2467	0.3412	0.2647	0.2969	**0.7191**	0.2386	0.2725	0.2724	0.3014	0.2712	0.2756
	Finger10	0.2838	0.2491	0.2631	0.2684	0.3019	0.3793	0.3535	0.3164	0.2395	**0.7750**	0.3609	0.3171	0.3329	0.2724	0.3118
	Finger11	0.2763	0.2736	0.2599	0.2714	0.3042	0.4476	0.3477	0.3576	0.2930	0.2787	**0.7982**	0.3494	0.3410	0.3179	0.3065
	Finger12	0.2850	0.2562	0.2931	0.2815	0.3393	0.4547	0.3434	0.3416	0.2778	0.2917	0.3288	**0.7348**	0.3818	0.3290	0.2833
	Finger13	0.3692	0.2802	0.2677	0.3087	0.2966	0.4900	0.3486	0.2921	0.2652	0.2916	0.2924	0.3747	**0.7768**	0.3351	0.2773
	Finger14	0.2812	0.2477	0.2856	0.2779	0.2637	0.4253	0.3212	0.3480	0.2780	0.2822	0.2622	0.3151	0.3491	**0.7493**	0.3325
	Finger15	0.3006	0.2316	0.2929	0.2934	0.3072	0.3912	0.3298	0.3264	0.2609	0.3004	0.3271	0.3070	0.3207	0.2723	**0.7251**

Table 2 Matching scores at $n_0 = 400$ (restoration from $1/(5 \times 5)$-subsampled images).

		Original Image														
		Finger01	Finger02	Finger03	Finger04	Finger05	Finger06	Finger07	Finger08	Finger09	Finger10	Finger11	Finger12	Finger13	Finger14	Finger15
Restored Image	Finger01	**0.7280**	0.2283	0.2398	0.2349	0.2787	0.3508	0.3062	0.3291	0.2410	0.3312	0.2607	0.2538	0.3159	0.2773	0.2755
	Finger02	0.2596	**0.6249**	0.2747	0.2548	0.2740	0.3343	0.2938	0.2867	0.2687	0.2740	0.2655	0.2836	0.2475	0.2614	0.2644
	Finger03	0.2392	0.2481	**0.7020**	0.2716	0.3008	0.3681	0.3186	0.2952	0.2623	0.2997	0.2747	0.3046	0.2949	0.2835	0.2703
	Finger04	0.2964	0.2713	0.2475	**0.6825**	0.2768	0.3705	0.3488	0.3128	0.2608	0.2878	0.2647	0.2955	0.2838	0.3048	0.3010
	Finger05	0.2783	0.2349	0.2613	0.2598	**0.6775**	0.3625	0.3266	0.3095	0.2876	0.2611	0.2685	0.2988	0.3143	0.2509	0.2593
	Finger06	0.2600	0.2390	0.2500	0.3289	0.3050	**0.6640**	0.3701	0.3090	0.2597	0.3402	0.2799	0.2864	0.3099	0.2625	0.2677
	Finger07	0.2635	0.2292	0.2395	0.2367	0.2835	0.3954	**0.6229**	0.3194	0.2489	0.2472	0.2925	0.2994	0.2713	0.2476	0.2375
	Finger08	0.3119	0.2480	0.2507	0.2761	0.3210	0.4130	0.3609	**0.7017**	0.2774	0.2970	0.2961	0.3212	0.3565	0.2849	0.3308
	Finger09	0.2546	0.2149	0.2513	0.2358	0.2755	0.3710	0.2927	0.2883	**0.6250**	0.2440	0.2883	0.2689	0.2547	0.2642	0.2581
	Finger10	0.3127	0.2242	0.2513	0.2825	0.2827	0.4180	0.3255	0.3430	0.2736	**0.6813**	0.2753	0.3064	0.2835	0.2750	0.2985
	Finger11	0.3067	0.2416	0.2687	0.2760	0.3309	0.3752	0.3121	0.3085	0.3037	0.3063	**0.6441**	0.3115	0.3262	0.3017	0.3065
	Finger12	0.3071	0.2530	0.2815	0.2822	0.3144	0.3896	0.3215	0.3567	0.2644	0.3212	0.3004	**0.7080**	0.3655	0.2958	0.2696
	Finger13	0.3058	0.2331	0.2597	0.2830	0.3019	0.4174	0.3043	0.3011	0.2494	0.2811	0.3061	0.3650	**0.7220**	0.3333	0.2893
	Finger14	0.2644	0.2411	0.2714	0.2756	0.2898	0.3862	0.3489	0.3203	0.2944	0.2610	0.2747	0.3398	0.3500	**0.6575**	0.2933
	Finger15	0.2901	0.2356	0.2642	0.2495	0.2760	0.4432	0.3007	0.3927	0.2841	0.2449	0.2890	0.3062	0.3852	0.2791	**0.6902**

Table 3 Matching scores at $n_0 = 400$ (restoration from $1/(6 \times 6)$-subsampled images).

		Original Image														
		Finger01	Finger02	Finger03	Finger04	Finger05	Finger06	Finger07	Finger08	Finger09	Finger10	Finger11	Finger12	Finger13	Finger14	Finger15
Restored Image	Finger01	**0.6166**	0.2569	0.2617	0.2694	0.2652	0.3358	0.2835	0.3079	0.2186	0.2549	0.3556	0.2814	0.2812	0.2333	0.2738
	Finger02	0.2526	**0.6589**	0.2514	0.2540	0.2705	0.2970	0.2903	0.3136	0.2553	0.2828	0.3199	0.3046	0.2491	0.2634	0.2848
	Finger03	0.2371	0.2690	**0.5449**	0.2714	0.2900	0.3382	0.2906	0.3183	0.2489	0.2704	0.2717	0.3191	0.2792	0.2458	0.3140
	Finger04	0.2820	0.2700	0.2798	**0.6380**	0.2879	0.3897	0.2946	0.3672	0.2673	0.2653	0.2651	0.2718	0.2961	0.3068	0.2978
	Finger05	0.2391	0.2498	0.2628	0.2670	**0.6503**	0.3657	0.3397	0.3152	0.2680	0.2706	0.3034	0.2893	0.2935	0.2793	0.2945
	Finger06	0.2548	0.2552	0.2669	0.2736	0.3042	**0.5856**	0.2985	0.2938	0.2586	0.2851	0.2406	0.3514	0.2640	0.2441	0.2754
	Finger07	0.2349	0.2256	0.2388	0.2858	0.2891	0.3386	**0.5162**	0.3134	0.2610	0.2824	0.2821	0.2698	0.2725	0.2624	0.2500
	Finger08	0.2815	0.2636	0.2531	0.2763	0.3188	0.3839	0.3491	**0.6784**	0.2625	0.2597	0.2654	0.3426	0.2921	0.2785	0.2845
	Finger09	0.2472	0.2157	0.2555	0.2649	0.2667	0.3048	0.2800	0.2763	**0.5386**	0.2556	0.2395	0.2752	0.2838	0.2674	0.2727
	Finger10	0.2718	0.2327	0.2454	0.2864	0.2942	0.3248	0.2921	0.3113	0.2588	**0.5952**	0.3201	0.2947	0.3220	0.2515	0.3219
	Finger11	0.2719	0.2749	0.2528	0.3008	0.3293	0.3892	0.3395	0.3334	0.2744	0.2872	**0.5957**	0.3446	0.3025	0.2649	0.3233
	Finger12	0.2792	0.2602	0.2619	0.2924	0.3330	0.3944	0.3000	0.3710	0.2598	0.2938	0.3036	**0.6241**	0.4110	0.2825	0.2930
	Finger13	0.2854	0.2593	0.2348	0.2811	0.3292	0.4772	0.2935	0.3427	0.2224	0.2707	0.3031	0.3726	**0.5973**	0.2512	0.2942
	Finger14	0.2742	0.2286	0.2514	0.3140	0.3252	0.3683	0.3041	0.3401	0.2797	0.2556	0.2887	0.3069	0.3574	**0.5407**	0.3056
	Finger15	0.2816	0.2335	0.2707	0.2451	0.3237	0.3718	0.2883	0.3009	0.2516	0.2889	0.2790	0.2927	0.3379	0.2913	**0.5062**

Table 4 Comparison of identification rate.

	Without Coarse-to-Fine Processing		With Coarse-to-Fine Processing	
Subsampling Rate	Number of Identified Samples	Identification Rate	Number of Identified Samples	Identification Rate
$1/(3 \times 3)$	15	100%	15	100%
$1/(3 \times 4)$	15	100%	15	100%
$1/(4 \times 4)$	15	100%	15	100%
$1/(4 \times 5)$	14	93%	15	100%
$1/(5 \times 5)$	11	73%	15	100%
$1/(5 \times 6)$	7	47%	15	100%
$1/(6 \times 6)$	6	40%	15	100%
$1/(6 \times 7)$	2	13%	14	93%
$1/(7 \times 7)$	0	0%	12	80%
$1/(7 \times 8)$	0	0%	5	33%
$1/(8 \times 8)$	0	0%	1	7%

for blurred fingerprint images. For subsampling rates higher than $1/(6{\times}6)$, it becomes increasingly difficult to find correct orientation masks. In this region, dedicated fingerprint models (such as deformable templates) may be required for further improvement of restoration performance.

5. Conclusion

This paper presents an application of DRDS to fingerprint image restoration. The adaptive DRDS combined with a coarse-to-fine orientation estimation technique can reconstruct complete fingerprint patterns even from $1/(6 \times 6)$-subsampled images. The proposed algorithm may be useful in many person identification applications based on fingerprint images.

References

[1] A.M. Turing, "The chemical basis of morphogenesis," Phil. Trans. R. Soc. London, vol.B237, pp.37–72, Aug. 1952.

[2] A.S. Sherstinsky and R.W. Picard, "M-lattice: From morphogenesis to image processing," IEEE Trans. Image Process., vol.5, no.7, pp.1137–1150, July 1996.

[3] K.R. Crounse and L.O. Chua, "Methods for image processing and pattern formation in cellular neural networks: A tutorial," IEEE Trans. Circuits Syst. I Fundam. Theory Appl., vol.42, no.10, pp.583–601, Oct. 1995.

[4] L. Goras, L.O. Chua, and L. Pivka, "Turing patterns in CNNs-Part II: Equations and behaviors," IEEE Trans. Circuits Syst. I Fundam. Theory Appl., vol.42, no.10, pp.612–626, Oct. 1995.

[5] K. Ito, T. Aoki, and T. Higuchi, "Digital reaction-diffusion system—A foundation of bio-inspired texture image processing," IEICE Trans. Fundamentals, vol.E84-A, no.8, pp.1909–1918, Aug. 2001.

[6] K. Takita, T. Aoki, Y. Sasaki, T. Higuchi, and K. Kobayashi, "High-accuracy image registration based on phase-only correlation and its experimental evaluation," Proc. 2002 IEEE International Symposium on Intelligent Signal Processing and Communication Systems (ISPACS), pp.86–90, Nov. 2002.

[7] http://www.aoki.ecei.tohoku.ac.jp/poc/

[8] L. Hong, Y. Wan, and A. Jain, "Fingerprint image enhancement: algorithm and performance evaluation," IEEE Trans. Pattern Anal. Mach. Intell., vol.20, no.8, pp.777–789, Aug. 1998.

[9] A. Almansa and T. Lindeberg, "Fingerprint enhancement by shape adaptation of scale-space operators with automatic scale selection," IEEE Trans. Image Process., vol.9, no.12, pp.2027–2042, Dec. 2000.

[10] J.D. Murray, Mathematical Biology, Springer-Verlag, Berlin, 1993.

Appendix: Pattern Formation Capability of DRDS

This appendix explains how to determine the parameter set of DRDS. To make a DRDS model generate stationary Turing patterns, we need to select the parameters of DRDS to satisfy the instability condition described in [5]. In practical situation, the above condition is ex-

```
% Spot pattern formarion with DRDS

% Initial settings
N = 64;                 % Image size
k1 = 2; k2 = 4;         % Parameters for Brusselator
D1 = 0.01; D2 = 0.05;   % Diffusion coefficients
T0 = 0.01; T1 = 0.53; T2 = 0.53;
                        % Sampling periods
l = [    0        1/T2^2        0;
     1/T1^2 -2*(1/T1^2+1/T2^2) 1/T1^2;
         0        1/T2^2        0    ];
% Initial morphogen distributions
x1 = rand(N+2,N+2)*2+k1-1;
x2 = ones(N+2,N+2)*k2/k1;
for i = 1:100
   for j = 1:50
      % Boundary condition
      x1(2:N+1,1:1) = x1(2:N+1,3:3);
      x1(2:N+1,N+2:N+2) = x1(2:N+1,N:N);
      x1(1:1,2:N+1) = x1(3:3,2:N+1);
      x1(N+2:N+2,2:N+1) = x1(N:N,2:N+1);
      x2(2:N+1,1:1) = x2(2:N+1,3:3);
      x2(2:N+1,N+2:N+2) = x2(2:N+1,N:N);
      x2(1:1,2:N+1) = x2(3:3,2:N+1);
      x2(N+2:N+2,2:N+1) = x2(N:N,2:N+1);
      % Brusselator reaction function
      R1 = T0*(k1-(k2+1)*x1+x1.^2.*x2);
      R2 = T0*(k2*x1-x1.^2.*x2);
      % DRDS computation
      x1 = x1+R1+D1*conv2(x1,l,'same');
      x2 = x2+R2+D2*conv2(x2,l,'same');
   end
   % Image display
   imshow(x1(2:N+1,2:N+1),[k1-1 k1+1]);
end
```

Fig. A· 1 MATLAB sample script of spot pattern formation using DRDS (Image Processing Toolbox is required).

pressed by a set of inequalities, and hence we can find only the ranges of parameters for possible pattern formation. Note that the above condition is not sufficient to ensure the generation of spatial patterns. In order to find the parameter set for DRDS that actually generates the desired patterns, we must carry out simulation experiments for the given DRDS model (since the system exhibits nonlinear dynamics). To give a hands-on example of how one observes the pattern formation with DRDS, Fig. A· 1 shows the MATLAB sample script for the DRDS defined by Eq. (2). Using this script, we can observe the 2D spot pattern development from the initial random concentration.

Koichi Ito received the B.E. degree in electronic engineering, and the M.S. degrees in information sciences from Tohoku University, Sendai, Japan, in 2000 and 2002, respectively. He is currently working toward the Ph.D. degree. His research interest includes non-linear digital signal processing and computer graphics. Mr. Ito received the Tohoku Section Presentation Award from Information Processing Society of Japan in 2000.

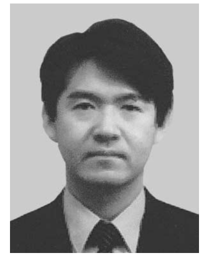

Takafumi Aoki received the B.E., M.E., and D.E. degrees in electronic engineering from Tohoku University, Sendai, Japan, in 1988, 1990, and 1992, respectively. He is currently a Professor of the Graduate School of Information Sciences at Tohoku University. For 1997–1999, he also joined the PRESTO project, Japan Science and Technology Corporation (JST). His research interests include theoretical aspects of computation, VLSI computing structures for signal and image processing, multiple-valued logic, and biomolecular computing. Dr. Aoki received the Outstanding Paper Award at the 1990, 2000 and 2001 IEEE International Symposiums on Multiple-Valued Logic, the Outstanding Transactions Paper Award from the Institute of Electronics, Information and Communication Engineers (IEICE) of Japan in 1989 and 1997, the IEE Ambrose Fleming Premium Award in 1994, the IEICE Inose Award in 1997, the IEE Mountbatten Premium Award in 1999, and the Best Paper Award at the 1999 IEEE International Symposium on Intelligent Signal Processing and Communication Systems.

Tatsuo Higuchi received the B.E., M.E., and D.E. degrees in electronic engineering from Tohoku University, Sendai, Japan, in 1962, 1964, and 1969, respectively. He is currently a Professor at Tohoku Institute of Technology. From 1980 to 1993, he was a Professor in the Department of Electronic Engineering at Tohoku University. He was a Professor from 1994 to 2003, and was Dean from 1994 to 1998 in the Graduate School of Information Sciences at Tohoku University. His general research interests include the design of 1-D and multi-D digital filters, linear time-varying system theory, fractals and chaos in digital signal processing, VLSI computing structures for signal and image processing, multiple-valued ICs, multiwave opto-electronic ICs, and biomolecular computing. Dr. Higuchi received the Outstanding Paper Awards at the 1985, 1986, 1988, 1990, 2000 and 2001 IEEE International Symposiums on Multiple-Valued Logic, the Outstanding Transactions Paper Award from the Society of Instrument and Control Engineers (SICE) of Japan in 1984, the Technically Excellent Award from SICE in 1986, and the Outstanding Book Award from SICE in 1996, the Outstanding Transactions Paper Award from the Institute of Electronics, Information and Communication Engineers (IEICE) of Japan in 1990 and 1997, the Inose Award from IEICE in 1997, the Technically Excellent Award from the Robotics Society of Japan in 1990, the IEE Ambrose Fleming Premium Award in 1994, the Outstanding Book Award from the Japanese Society for Engineering Education in 1997, the Award for Persons of scientific and technological merits (Commendation by the minister of state for Science and Technology), the IEE Mountbatten Premium Award in 1999 and the Best Paper Award at the 1999 IEEE International Symposium on Intelligent Signal Processing and Communication Systems. He also received the IEEE Third Millennium Medal in 2000. He received the fellow grade from IEEE, IEICE, and SICE.